Difference frequency generation in optically poled silicon nitride waveguides

Ezgi Sahin[1], Boris Zabelich[1], Ozan Yakar[1], Edgars Nitiss[1], and Camille-Sophie Brès[1,*]

[1]Ecole Polytechnique Fédérale de Lausanne, Photonic Systems Laboratory, 1015 Lausanne Switzerland

ABSTRACT

All-optical poling leads to an effective second-order nonlinearity ($\chi^{(2)}$) in centrosymmetric materials without the need for sophisticated fabrication techniques or material processing, through the periodic self-organization of the charges. The absence of the inherent $\chi^{(2)}$ in prevailing silicon-based platforms can be surmounted through all-optical poling. Using the induced effective $\chi^{(2)}$ in silicon nitride (Si_3N_4) waveguides, nonlinear frequency up-conversion processes, such as second-harmonic generation, were previously demonstrated on Si_3N_4. Here, we report near- and non-degenerate difference-frequency generation in all-optically poled Si_3N_4 waveguides. We show the agreement between the theory and the measurements and optimize achievable QPM bandwidth range, reaching conversion efficiency of 1 %/W.

Keywords: Second-order nonlinearity, integrated optics, all-optical poling, difference-frequency generation.

1. INTRODUCTION

Silicon nitride (Si_3N_4), with tuneable material composition and well-developed CMOS-compatible material processing techniques, is heading towards being the bridging material platform for passive devices, nonlinear components, and high-performance electro-optical modulators.[1,2] Nevertheless, Si_3N_4 suffers from the low second-order susceptibility, $\chi^{(2)}$, due to its centrosymmetric nature, which inhibits three-photon mixing processes such as second harmonic generation (SHG), sum- frequency generation (SFG), and difference frequency generation (DFG).

Lately, researchers efforts are being directed to realizing $\chi^{(2)}$ processes on integrated platforms. Forcing the symmetry breaking can induce an effective second-order susceptibility in centrosymmetric materials and compensate the absence of the inherent $\chi^{(2)}$ nonlinearity. In silicon-based integrated platforms, second order nonlinear processes has been demonstrated through quasi-phase-matching (QPM) via using resonant structures[3,4] or poling techniques such as all-optical poling[5–7] and electric-field induced second harmonic generation (EFISHG).[8] All-optical poling does not require complex fabrication techniques or additional material processing such as electrode deposition or intricate resonator designs to achieve QPM, making it straightforward to implement. Using the effective $\chi^{(2)}$ inscribed in the all-optically poled waveguides, second-order nonlinear frequency upconversion processes; SHG[5,6] and SFG[9] were previously demonstrated on Si_3N_4, whereas thus far, DFG has remained elusive in silicon-based integrated platforms, though it is a crucial process for generating coherent light at long wavelength, especially the middle-infrared (mid-IR).

Here, we demonstrate DFG on Si_3N_4 waveguides through all-optical poling. We present the experimental results of conversion efficiency (CE) by changing pump wavelength along with the theoretical calculations that show an excellent agreement with measurements. The scaling of the idler power with respect to the pump and signal powers is also investigated.

E-mail: camille.bres@epfl.ch

2. RESULTS

2.1 Near-degenerate DFG

To induce the effective $\chi^{(2)}$ needed for the DFG, the Si_3N_4 waveguides are all optically poled. The all-optical poling was realized at 30^{o}C, at 1555 and 1560 nm for waveguides with cross-sections 1.8 x 0.75 μm and 2.0 x 0.75 μm, respectively. The temperature was controlled and maintained via a PID controller, a Peltier element and a temperature transducer.[6] High peak power nanosecond pulses were injected into the waveguide to alter the position of the charges along the waveguide in a spatially periodic fashion. The DC field created by this periodicity, which is needed for the QPM, induces the effective $\chi^{(2)}$. A more comprehensive description of the poling process as well as the experimental details were presented before and can be found in Refs. 6, 10.

The effective $\chi^{(2)}$ induced by the all-optical poling is derived from the SHG measurements throughout the telecommunication C-band. The spectral dependence of CE for the SHG obtained through this measurement is analyzed through a least-squares fit, allowing us to obtain the values of $\chi^{(2)}_{eff}$ and the grating length L, further details on extracting these parameters can be found elsewhere.[6] $\chi^{(2)}_{\text{eff}}$ values are estimated in the 0.06 - 0.19 pm/V range, in agreement with previous reported values. We use these parameters, $\chi^{(2)}_{eff}$ and L, to calculate the spectral dependence of QPM for DFG process.

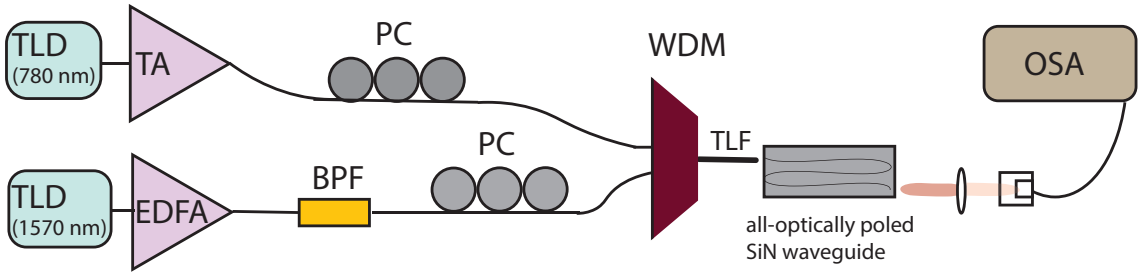

Figure 1. Schematic of the DFG setup consisting of TLDs (tunable laser diodes), EDFA (Erbium-doped fiber amplifier), TA (Tapered Amplifier), BPF (bandpass filter), PC (polarization controller), WDM (wavelength division multiplexer), TLF (tapered lensed fiber) and OSA (optical spectrum analyzer).

The optical setup used to realize near-degenerate DFG in poled waveguides is shown in Figure 1. Tunable laser diodes cascaded with amplifiers are used for both pump and signal arm. The signal is then filtered using a bandpass filter to increase the visibility of idler via reducing the amplifier induced noises. The waveguide is birefringent and was poled to operate in either TE or TM polarization, therefore both pump and signal arms include a polarization controller.

In our experiments, we kept the signal fixed while changing the pump wavelength to understand and showcase the DFG behavior according to QPM's spectral dependence induced by all-optical poling. Figure 2 shows the idlers generated at the telecommunication C-band at 25^{o}C in TE polarization. Figure 3(a) demonstrates the CE of DFG at the same temperature for the waveguide with cross-section 1.8 x 0.75 μm .

The experimental conversion efficiency is calculated by CE= $P_{\text{i}}/P_{\text{s}}P_{\text{P,dfg}}$, with P_{i}, P_{s} and $P_{\text{P,dfg}}$ the idler, signal and pump powers. The insertion loss per facet is 3 dB for telecommunication band and 6.5 dB for visible light. The pump was varied between 775 nm to 781 nm at 0.2 nm increments. With our visible source, we could not reach a wide range of wavelengths to show the entire theoretically expected sinc-square like curve in TE polarization.

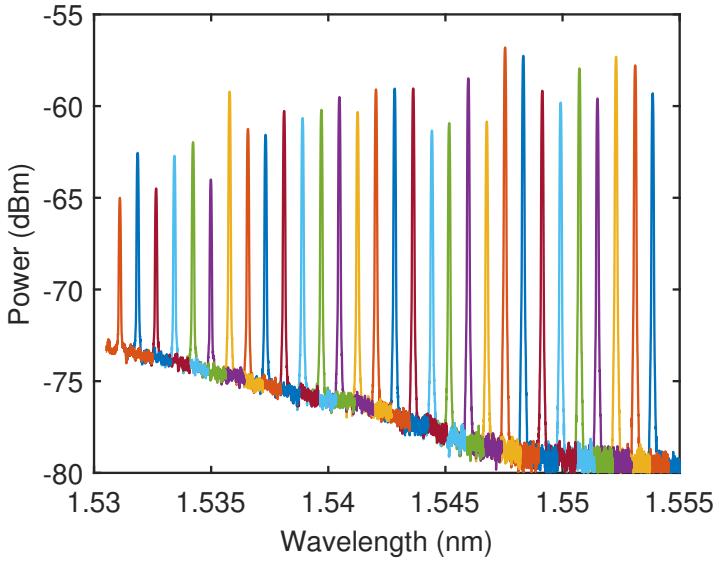

Figure 2. Near-degenerate DFG in optically poled 1.8 x 0.75 μm^2 Si_3N_4 waveguide, idlers spectra generated from a 1570 nm signal and a pump tuned from 775 to 781 nm in 0.2 nm steps at 25°C for TE poling.

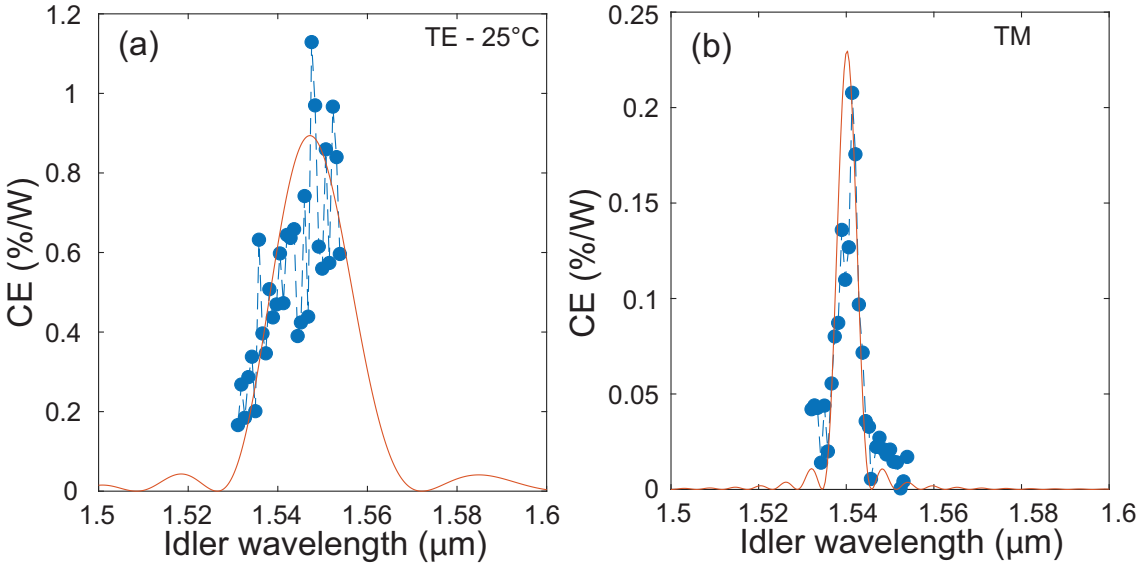

Figure 3. (a) DFG theoretical (full lines) and measured CE (dots) as a function of idler wavelength for chip temperature 25°C at TE. (b) DFG theoretical and measured CE as a function of idler wavelength for TM.

The theoretical DFG CE in all optically poled waveguides can be calculated based on the phase-matching conditions. The phase mismatched $\Delta\beta$ is given by:

$$\Delta\beta = 2\pi\left(\frac{n_{\text{eff}}^{\text{P,dfg}}}{\lambda_{\text{P,dfg}}} - \frac{n_{\text{eff}}^{\text{s}}}{\lambda_{\text{s}}} - \frac{n_{\text{eff}}^{\text{i}}}{\lambda_{\text{i}}} - \frac{1}{\Lambda}\right) \tag{1}$$

where $n_{\text{eff}}^{\text{P,dfg}}$, $n_{\text{eff}}^{\text{s}}$, $n_{\text{eff}}^{\text{i}}$, $\lambda_{\text{P,dfg}}$, λ_{s} and λ_{i} are the effective refractive indices and wavelengths of the DFG pump, signal and idler, respectively. The CE is then given by:

$$\text{CE} = \frac{2\pi^2\chi_{\text{eff}}^2}{n_{\text{eff}}^{\text{P,dfg}} n_{\text{eff}}^{\text{s}} n_{\text{eff}}^{\text{i}} c\epsilon_0 \lambda_{\text{i}}^2}\frac{L^2}{A_{\text{eff}}}\frac{\sin^2\left(\frac{\Delta\beta L}{2}\right)}{\left(\frac{\Delta\beta L}{2}\right)^2} \tag{2}$$

where $\chi_{\text{eff}}^{(2)}$ and L are extracted from the experimentally measured SHG CE as previously mentioned, and A_{eff} is the effective area calculated as $A_{\text{eff}} = A_{\text{eff}}^{\text{P,dfg}} A_{\text{eff}}^{\text{s}}/A_{\text{eff}}^{\text{i}}$ using modal simulations. The theoretically expected curves are shown in Figure 3 alongside the experimental data. The data and theoretical curves are in excellent agreement. To show the entire phase-matching curve, we poled the same waveguide in TM polarization which has a much narrower bandwidth than in the TE case owing to larger difference in terms of effective refractive index between idler, signal and pump, Figure 3(b) shows the full CE bandwidth in TM.

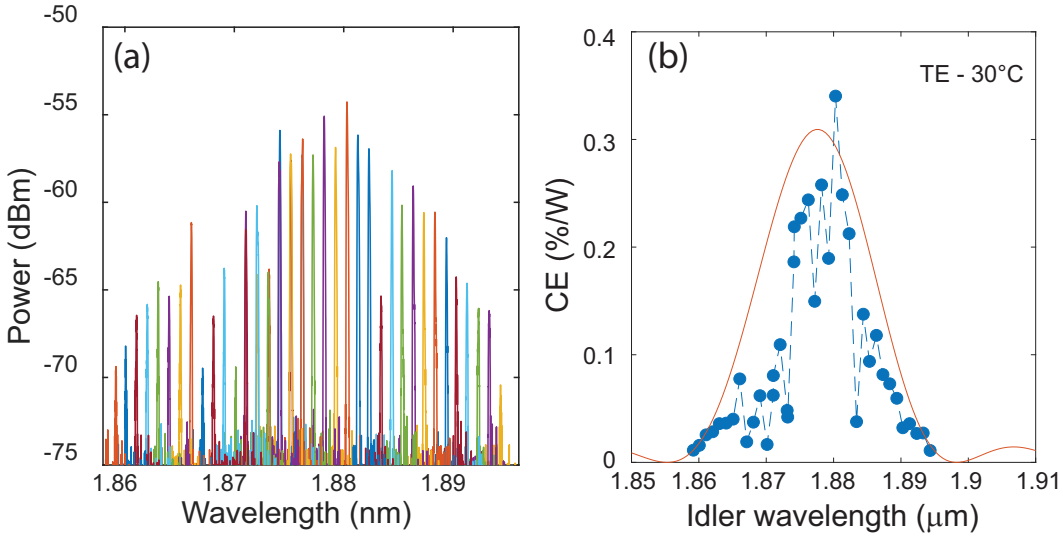

Figure 4. Non-degenerate DFG in optically poled Si_3N_4 waveguide with cross-section of 2.0 x 0.75 μm^2 (a) spectra of idlers generated by mixing 1535 nm signal and pump ranging from 841 to 848 nm at 30°C. (b) DFG theoretical (full lines) and measured CE (dots) as a function of idler wavelength for chip temperature 30°C.

2.2 Non-degenerate DFG

Next, we aimed to push the idler towards higher wavelengths. We simulated the expected DFG efficiency to identify if there is a QPM region for another pump laser available in our laboratory. For the waveguide with a cross-section of 2.0 × 0.75 μm, we identified a QPM region for pump wavelengths around 840 nm, where the waveguide is poled at 1560 nm, and the signal is at 1535 nm. After poling the waveguide 30^{o}C to engrave the grating needed for the QPM of DFG. Idlers measured by changing the pump wavelength can be seen in Figure 4(a). The simulated and the measured CE show a good agreement, as seen in Figure 4(b).

To investigate the scaling rules of DFG, we measured the power dependence of the output idler as a function of the pump power. Figure 5(a) shows the on-chip idler power scaling linearly to the coupled input pump power. We could not increase the power beyond the measurements presented here due to the limited output power of

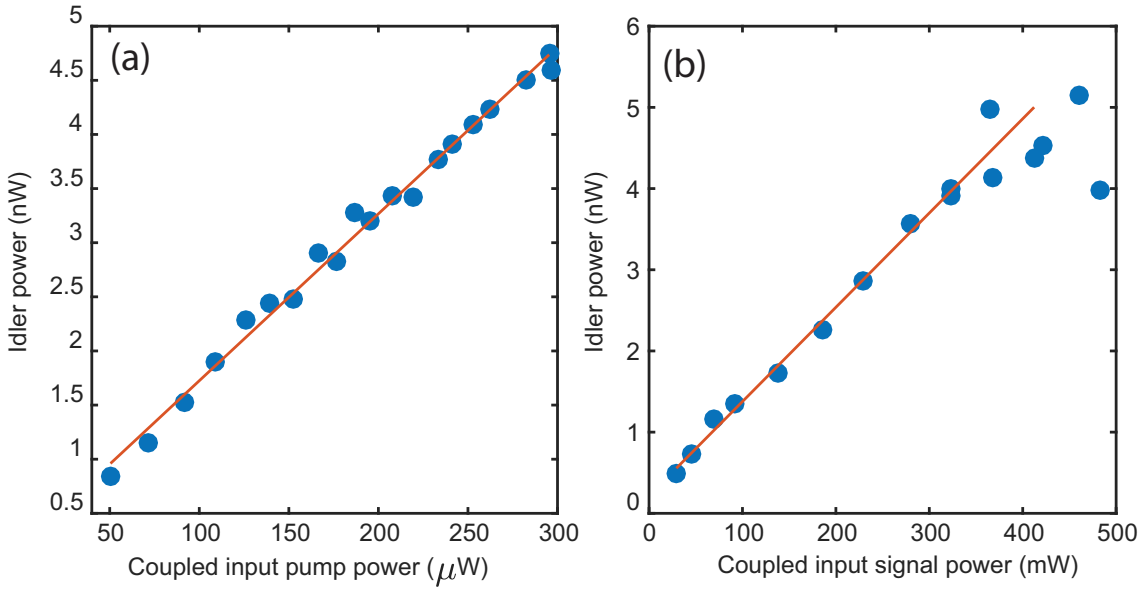

Figure 5. Non-degenerate DFG idler scaling with the increased power of: (a) the 840 nm pump and (b) the 1535 nm signal. Blue dots are the measurements and the lines are the linear fit as a visual guide.

the 840 nm laser available in our laboratory. We demonstrated the expected linear relationship in this low power region; if the power is increased further, it is expected to see the erasure of the grating.[11]

Figure 5(b) shows the scaling of the idler power as the coupled input signal power increases. Idler power increases linearly until the coupled input signal power is around 400 mW. The linear relationship does not continue beyond this point, and we see that the measurements with the highest powers do not result in idler powers as high as expected. When the coupled input signal power is 368 mW, for every pump photon, there are more than three orders of magnitude signal photons. Therefore, the reduction in CE can be credited to the excessive number of signal photons compared to the pump photons.[12]

3. DISCUSSION AND CONCLUSION

DFG for realizing mid-IR sources instead of wide-spanning supercontinuum generation has the potential to eliminate the need for femtosecond sources and lessen the dependency for ultrashort pulses, alongside extending the wavelength range, to generate mid-IR wavelengths on-chip. DFG has been investigated in $LiNbO_3$ for a wide range of mid-IR idler wavelengths,[13–15] and our results can pave the way for DFG applications in silicon-based platforms.

In this work, we presented near- and non-degenerate DGF on Si_3N_4 platform. Alongside the experimental demonstrations, we show the CE's theoretical expectations based on the simulations of the effective refractive index and the extracted inscribed grating parameters through the SHG characterization. We also investigated the DFG scaling rules. This research will pave the way towards simple and compact tunable coherent light sources at large processing yields for the key operation wavelengths of mid-IR.

ACKNOWLEDGMENTS

The funding was provided by ERC grant PISSARRO (ERC-2017-CoG 771647).

REFERENCES

[1] Blumenthal, D. J., Heideman, R., Geuzebroek, D., Leinse, A., and Roeloffzen, C., "Silicon Nitride in Silicon Photonics," *Proceedings of the IEEE* **106**(12), 2209–2231 (2018).

[2] Moss, D. J., Morandotti, R., Gaeta, A. L., and Lipson, M., "New CMOS-compatible platforms based on silicon nitride and Hydex for nonlinear optics," (aug 2013).

[3] Levy, J. S., Foster, M. A., Gaeta, A. L., and Lipson, M., "Harmonic generation in silicon nitride ring resonators," *Opt. Express* **19**, 11415–11421 (Jun 2011).

[4] Ning, T., Pietarinen, H., Hyvärinen, O., Kumar, R., Kaplas, T., Kauranen, M., and Genty, G., "Efficient second-harmonic generation in silicon nitride resonant waveguide gratings," *Opt. Lett.* **37**, 4269–4271 (Oct 2012).

[5] Billat, A., Grassani, D., Pfeiffer, M. H., Kharitonov, S., Kippenberg, T. J., and Brès, C.-S., "Large second harmonic generation enhancement in si_3n_4 waveguides by all-optically induced quasi-phase-matching," *Nature Communications* **8**, 1–7 (2017).

[6] Nitiss, E., Zabelich, B., Yakar, O., Liu, J., Wang, R. N., Kippenberg, T. J., and Brès, C.-S., "Broadband quasi-phase-matching in dispersion-engineered all-optically poled silicon nitride waveguides," *Photon. Res.* **8**, 1475–1483 (Sep 2020).

[7] Hickstein, D. D., Carlson, D. R., Mundoor, H., Khurgin, J. B., Srinivasan, K., Westly, D., Kowligy, A., Smalyukh, I. I., Diddams, S. A., and Papp, S. B., "Self-organized nonlinear gratings for ultrafast nanophotonics," *Nature Photonics* **13**, 494–499 (2019).

[8] Timurdogan, E., Poulton, C. V., Byrd, M. J., and Watts, M. R., "Electric field-induced second-order nonlinear optical effects in silicon waveguides," *Nature Photonics* **11**, 200–2006 (2017).

[9] Grassani, D., Pfeiffer, M. H. P., Kippenberg, T. J., and Brès, C.-S., "Second- and third-order nonlinear wavelength conversion in an all-optically poled Si_3N_4 waveguide," *Opt. Lett.* **44**, 106–109 (Jan 2019).

[10] Nitiss, E., Liu, T., Grassani, D., Pfeiffer, M., Kippenberg, T. J., and Brès, C.-S., "Formation rules and dynamics of photoinduced $\chi^{(2)}$ gratings in silicon nitride waveguides," *ACS Photonics* **7**(1), 147–153 (2020).

[11] Ouellette, F., Hill, K. O., and Johnson, D. C., "Light-induced erasure of self-organized $\chi^{(2)}$ gratings in optical fibers," *Opt. Lett.* **13**, 515–517 (Jun 1988).

[12] Wang, Y., Ghotbi, M., Das, S., Dai, Y., Li, S., Hu, X., Gan, X., Zhao, J., and Sun, Z., "Difference frequency generation in monolayer mos2," *Nanoscale* **12**, 19638–19643 (2020).

[13] Chou, M. H., Hauden, J., Arbore, M. A., and Fejer, M. M., "1.5-µm-band wavelength conversion based on difference-frequency generation in $LiNbO_3$ waveguides with integrated coupling structures," *Opt. Lett.* **23**, 1004–1006 (Jul 1998).

[14] Tadanaga, O., Yanagawa, T., Nishida, Y., Miyazawa, H., Magari, K., Asobe, M., and Suzuki, H., "Efficient 3-μm difference frequency generation using direct-bonded quasi-phase-matched $LiNbO_3$ ridge waveguides," *Applied Physics Letters* **88**(6), 061101 (2006).

[15] Hofmann, D., Schreiber, G., Haase, C., Herrmann, H., Grundkötter, W., Ricken, R., and Sohler, W., "Quasi-phase-matched difference-frequency generation in periodically poled Ti:$LiNbO_3$ channel waveguides," *Opt. Lett.* **24**, 896–898 (Jul 1999).